Coupled dark energy: Parameter constraints from *N*-body simulations

A.V. Macciò,[1] C. Quercellini,[2,3] R. Mainini,[1] L. Amendola,[2] and S.A. Bonometto[1]
[1]*Università di Milano Bicocca and INFN, Sezione di Milano, Piazza della Scienza 3, 20126 Milano, Italy*
[2]*INAF/Osservatorio Astronomico di Roma, Via Frascati 33, 00040 Monte Porzio Catone, Italy*
[3]*Università di Roma – Tor Vergata, Via della Ricerca Scientifica 1, 00133 Roma, Italy*
(Received 26 September 2003; published 25 June 2004)

We investigate cosmologies where dark matter (DM) is coupled to dark energy (DE), through *N*-body simulations. The dark-dark coupling introduces two novel effects in particle dynamics: (i) DM particle masses vary with time; (ii) gravity between DM particles is ruled by a constant G^*, greater than Newton's constant G, holding in other two-body interactions. Hence, DM particle dynamics violates the equivalence principle and, as a consequence, baryons and DM particle distributions develop a large scale bias. Here we focus on DE models with Ratra-Peebles (RP) potentials. The dark-dark coupling is set in a parametric range compatible with background and linear dynamics. We find that nonlinear dynamics puts additional constraints on the coupling parameter. They mostly arise from cluster density profiles that we find to yield higher concentrations in coupled RP models, with respect to (uncoupled) dynamical DE cosmologies. Such an enhancement, although being a strong effect in some coupling parameter range, leads to acceptable observables for a significant range of values of the coupling parameter. We also analyze the expected cluster *mass function* and the DM-baryon bias in nonlinear conditions, finding them compatible with data. With the above restrictions, coupled DE models with a RP potential are therefore consistent with cosmological nonlinear observables. As a general conclusion, we confirm that cosmologies with a suitable dark-dark coupling are viable theories.

DOI: 10.1103/PhysRevD.69.123516 PACS number(s): 98.80.Cq, 95.35.+d

I. INTRODUCTION

The nature of dark energy (DE) is one of the main puzzles of cosmology. DE was first required by supernova type (Ia) (SNIa) data [1], but with a *flat* universe with $\Omega_m \simeq 0.3$, $h \simeq 0.7$, and $\Omega_b h^2 \simeq 0.02$, is also favored by cosmic microwave background (CMB) and large scale structure (LSS) observations [2] ($\Omega_{m,b}$ are matter and baryon density parameters; h is the Hubble parameter in units of 100 km/s/Mpc).

DE could be a false vacuum; from the expression of its stress-energy tensor, $T^{(DE)}_{\mu\nu} = \Lambda g_{\mu\nu}$ (Λ is a positive constant and $g_{\mu\nu}$ is the metric tensor), one immediately appreciates that its pressure and energy density (p_{DE} and ρ_{DE}) have the ratio $w = -1$. A false vacuum, however, requires severe fine-tuning at the end of the electroweak (EW) transition. Otherwise, DE could be a scalar field ϕ self-interacting through a potential $V(\phi)$. Then

$$\rho_{DE} = \dot{\phi}^2/2a^2 + V(\phi), \quad p_{DE} = \dot{\phi}^2/2a^2 - V(\phi) \tag{1}$$

(here the overdots indicate differentiation with respect to the conformal time τ and a is the scale factor, so that the background metric reads $ds^2 = a^2[-d\tau^2 + \delta_{ij} dx_i dx_j]$, $i,j = 1,3$). However, if the kinetic component $\rho_k(\phi) \equiv \dot{\phi}^2/2a^2$ approaches the potential component $V(\phi)$, p_{DE} vanishes and the scalar field ϕ behaves as CDM (cold dark matter). This happens, e.g., in the well known case of axion DM. But, even for lower ρ_k, if $1/2 < \rho_k/V < 1$, it is $-1/3 < w < 0$ and the model, at most, approaches an open CDM behavior. The relevant domain is attained when $\rho_k/V \ll 1/2$, although keeping a state parameter $w > -1$. Then ϕ approaches a CDM with a cosmological constant (ΛCDM) behavior and is currently dubbed *dynamical* DE [3–5].

The conceptual contiguity between DM and dynamical DE suggests that they may not be disjoint entities. If so, one could hopefully ease the cosmic coincidence problem, i.e., that DM and DE densities, after being different by orders of magnitude for most of cosmic history, approach equal values only in today's Universe. The simplest way to deal with this idea amounts to admitting an interaction between DM and DE [6]. The coupling introduces an extra attractive force on DM particles, but not on baryons; this scalar gravity therefore violates the equivalence principle, but for the DM component only, which is not directly observable. We shall refer to these models, where DM and dynamical DE interact, as *coupled* DE models. Different models were also proposed that introduce a direct link between DM and DE, invoking a unified model (e.g., [7]) or condensation mechanisms [8]. Such models will not be considered here. In a number of papers [3,4,9,10], it has been shown that, besides being acceptable at a particle level, all cosmological data, predictable within a linear theory, can be suitably fitted by coupled DE models.

An open question, then, concerns the emergence of nonlinear structures in these models and how easy it is to fit observed LSS data with predictable features. In this work we deal with this problem by using *N*-body simulations of coupled DE models for DE self-interacting through a Ratra-Peebles (RP) potential [11]:

$$V(\phi) = \Lambda^{4+\alpha}/\phi^{\alpha}. \tag{2}$$

Once the exponent α and the DE density parameter Ω_{DE} are fixed, the energy scale Λ is set. This self-interaction allows $w \ll -1/3$, if Λ is sufficiently low.

Let us outline here that our nonlinear treatment sets precise constraints on coupled DE parameters. A wide parameter

TABLE I. Simulation details.

Model	α	β	Box size (h^{-1} Mpc)	No. of particles	Mass resolution ($h^{-1}M_\odot$)	Force resolution (h^{-1} kpc)
RP_1	0.143	0.05	80	128^3	2.0×10^{10}	5
RP_2	0.143	0.10	80	128^3	2.0×10^{10}	5
RP_3	0.143	0.15	80	128^3	2.0×10^{10}	5
RP_4	0.143	0.2	80	128^3	2.0×10^{10}	1.2
RP_5	0.143	0.25	80	128^3	2.0×10^{10}	1.2
RP_6	2.0	0.15	80	128^3	2.0×10^{10}	5
ΛCDM	0	0	80	128^3	2.0×10^{10}	5

space however remains where, apparently, these models fit LSS data as well as those with (uncoupled) dynamical DE. Coupled DE with a RP potential, however, allows no improvement of such a fit. The above motivations for coupled DE [12], however, remain and, altogether, the nonlinear test is successfully passed and is useful to better define the allowed parameter space.

N-body simulations of models with (uncoupled) dynamical DE were recently performed [13–15]. Here we follow the same pattern as [14] and use the program ART [16] providing, first of all, a fair dependence of the matter density parameter Ω_m on the scale factor a. To our knowledge, this is the first time an *N*-body simulation with species-dependent scalar gravity has been carried out. Our conclusions are based on simulations of a variety of models with different RP slopes α and coupling parameters β. Let us list them here. First of all, we test two α slopes 0.143 and 2. The latter value approaches the greatest value for which agreement with CMB observations is granted [3]. This is the range of RP models which are most distant from the ΛCDM. We also explored a wide set of β couplings, ranging from 0.05 to 0.25. All simulations were performed starting from the same random numbers and, for the sake of comparison, we also run a ΛCDM simulation starting from such random numbers. The other parameters were set to values chosen in agreement with recent CMB experiments [2]: $\Omega_c h^2=0.15$, $\Omega_b h^2=0.01$, $h=0.7$ [Ω_c is the (cold) DM density parameter]. All models are normalized so that $\sigma_8=0.75$ today, to match both CMB data and the observed cluster abundance [17]. Further details on the simulation performed are listed in Table I.

For all these models we also run a high-resolution simulation of a single halo, with a mass resolution of $2.5\times10^9 h^{-1}M_\odot$ and a force resolution of $1.2h^{-1}$ kpc.

In the next section we discuss the linear and postlinear aspects of coupled DE, explaining, in particular, how $\Omega_m(a)$ is obtained and used. In Sec. III we focus on the Newtonian regime for coupled DE models and describe the different gravitation of baryons and DM. In Sec. IV, we implement these prescriptions in the numerical code, so explaining what further modifications ART needs to deal with coupled DE. Section V is then devoted to illustrating the results while, in Sec. VI, we draw our conclusions.

II. BACKGROUND EXPANSION IN MODELS WITH COUPLED DARK ENERGY

Quite in general, energy density and pressure, for each component, in models with dynamical DE, are obtainable from the stress-energy tensors $T^{(c,b,r,\phi)}_{\mu\nu}$ (for CDM, baryons, radiation, and DE, respectively; radiation includes neutrinos). General covariance requires that the sum $T_{\mu\nu}$ of these four tensors satisfies the *continuity equation*

$$T^{\mu}_{\nu;\mu}=0, \tag{3}$$

and, although this is true if all tensors satisfy it separately, such a requirement is not necessary; e.g., when we deal with fluctuations before hydrogen recombination, only the sum of the baryon and e.m. radiation tensors satisfies it. In a similar way, if DE and DM interact, we can have that

$$T^{(\phi)\ \mu}_{\nu;\mu}=\sqrt{\frac{16\pi G}{3}}\beta T^{(c)}\phi_{;\nu}, \tag{4}$$

$$T^{(c)\ \mu}_{\nu;\mu}=-\sqrt{\frac{16\pi G}{3}}\beta T^{(c)}\phi_{;\nu}$$

(here $T^{(c)}$ is the trace of the CDM stress-energy tensor), and the sum of DM and DE satisfies Eq. (3). No analogous interaction should involve baryons, for which we assume that $T^{(b)\ \mu}_{\nu;\mu}=0$; in fact, experimental and observational constraints restrict a hypothetical DE-baryon coupling to $\beta_b<0.01$ [18]; also radiation cannot be involved, as the trace of its stress-energy tensor vanishes because of its equation of state.

The particular form of the coupling (4) reduces to Brans-Dicke scalar gravity upon a conformal transformation (see, e.g., [12,18–20]), generating terms of the form $f(\phi,R)$ in the so-called Jordan frame Lagrangian. In this frame one can generate species-dependent interactions by coupling matter to metrics with suitably defined conformal factors. Couplings of the above form are expected in any low-energy limit of a multidimensional Lagrangian, where the dilaton plays the role of the scalar field. Models based on such limits have been presented in the literature (see, e.g., [21]). A scalar coupling is therefore an expected feature of any extension of Einstein's gravity.

The explicit expression of the continuity equations is

$$\ddot{\phi}+2\mathcal{H}\dot{\phi}+a^2V_{,\phi}=\sqrt{16\pi G/3}\beta a^2\rho_c, \tag{5}$$

$$\dot{\rho}_c+3\mathcal{H}\rho_c=-\sqrt{16\pi G/3}\beta\rho_c\dot{\phi}, \tag{6}$$

$$\dot{\rho}_b+3\mathcal{H}\rho_b=0, \tag{7}$$

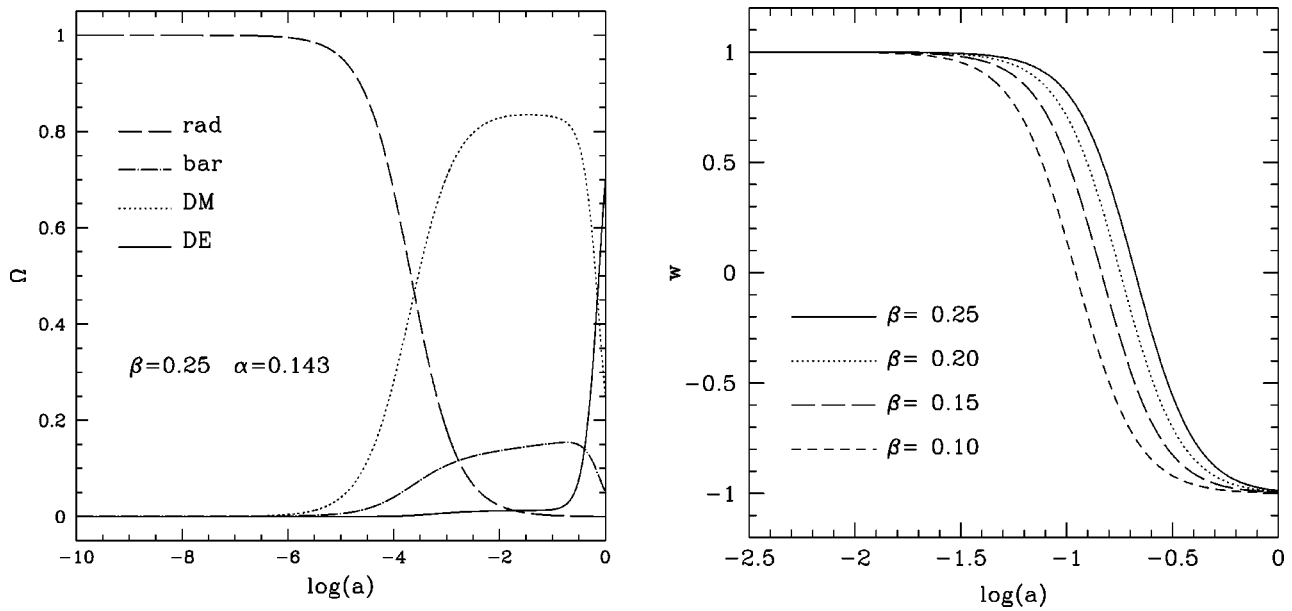

FIG. 1. Left panel: density parameters for radiation, baryons, DM, and DE. Just after radiation equivalence, a DE plateau occurs, due to the dark-dark coupling. In the text this plateau is denominated the ϕ-MDE stage. Right panel: evolution of the state parameter w for different values of β.

$$\dot{\rho}_r + 4\mathcal{H}\rho_r = 0. \tag{8}$$

Here $\mathcal{H}=\dot{a}/a$ is the conformal Hubble parameter. The dimensionless constant β^2 can be seen as the ratio of the DE-DM interaction with respect to gravity [6,18]. In these models, after *equivalence*, the world passes through three different expansion regimes, denominated (i) matter dominated expansion ϕ-(MDE), (ii) the tracking phase [5], and (iii) a final global attractor.

Immediately after equivalence, the world enters a ϕ-MDE stage (see [6]), not far from the matter dominated expansion, although one should not neglect a small correction, proportional to β, due to the kinetic term $\rho_k(\phi)$. $V(\phi)$, instead, is negligible and, accordingly, the correction is independent of the potential shape. By solving the Friedmann equation we find that

$$a \propto t^{4/(6+4\beta^2)}, \tag{9}$$

i.e., that the scale factor grows more slowly than in a pure MDE (in Sec. V B, we shall see that, on the contrary, the perturbation growth is enhanced during this stage). During the ϕ-MDE stage, $V(\phi)$ gradually increases and, eventually, approaches and exceeds $\rho_k(\phi)$; then the world enters the *tracking phase*, whose details depend on the potential shape; for most potentials, this phase ends up in a *global attractor*, when the DE density overwhelms DM and any other densities.

Along the expansion history, the scaling of ρ_c (DM density) is modified with respect to the uncoupled case and reads

$$\rho_c = \frac{\rho_{oc}}{a^3} e^{-\sqrt{16\pi G/3}\beta(\phi-\phi_0)}; \tag{10}$$

here the subscript o indicates value at the present time τ_o, while we take $a_o=1$. Meanwhile, the baryon density grows as a^{-3}, as usual.

In the next section we shall see that these behaviors strongly affect the fluctuation growth, even in the Newtonian regime. Figure 1 (left panel) shows the different trends of the density parameters for two different values of the coupling parameter β. The three stages of the background evolution are clearly visible. For the sake of completeness we also report in Fig. 1 (right panel) the a dependence of the state parameter w for different value of β. Notice that, for RP models with a low α, the value of the state parameter has been quite close to -1, since a redshift ~ 3–4.

Throughout these stages, however, according to the Friedman equations, the following relation holds [13]:

$$\frac{dt}{da} \equiv \chi(a) = H_o^{-1} \sqrt{\frac{a\Omega_b(a)}{\Omega_b(a_o)}}. \tag{11}$$

Therefore, once the a dependence of the baryon density parameter is given, all derivatives with respect to time can be easily converted into derivatives with respect to the scale factor. This relation will be used in the implementation of the ART program.

III. DYNAMICS IN THE NEWTONIAN REGIME

Let us now consider density fluctuations and discuss their evolution. First of all, the conformal metric must be modified to take into account the local gravitational fields and, in the absence of anisotropic stresses, reads

$$ds^2 = a^2[-(1+2\Phi)d\tau^2 + (1-2\Phi)dx_i dx^j],$$

Φ being the gravitational potential. Let us use $\alpha = \log a$ as the independent variable, instead of τ. Differentiation with respect to α will be indicated by a prime. Attention must be paid not to confuse this α with the exponent in the RP potential expression. As usual, fluctuations are expanded in Fourier components; let us then consider a component of wave number k and define $\lambda = \mathcal{H}/k$.

Baryons and CDM will be considered as fluids; fluctuations will then be characterized by density fluctuations

$$\delta^{c,b} = \delta\rho_{c,b}/\rho_{c,b} \tag{12}$$

(c,b stand for CDM and baryons) and velocity fields $v_i^{c,b} \equiv dx_i/d\tau$, from which we build the scalar variables

$$\theta^{c,b} = i\frac{k_i v^{c,b}{}_i}{\mathcal{H}}. \tag{13}$$

Scalar field fluctuations ($\delta\phi$) will then be described by the variable

$$\varphi = \sqrt{\frac{3}{4\pi G}}\delta\phi. \tag{14}$$

In dealing with fluctuation evolution well after recombination, we shall neglect the radiation component.

Taking into account density inhomogeneities, Eq. (3) yields the dependence of $\delta^{c,b}$ and $\theta^{c,b}$ on the scale factor a. The Friedmann equation will then be used to obtain the dependence on time. We shall omit here the general form of these equations (see [10]), and will write them in the Newtonian limit, i.e., for small scales (in comparison with the horizon scale $\sim H^{-1}$) and small velocities (with respect to c).

The former condition tells us to consider the lowest-order terms in λ; in this limit, the gravitational potential satisfies equations that can be written in a simpler form by defining the function $f(\phi)$ according to

$$V(\phi) = A\exp\left[\sqrt{\frac{16\pi G}{3}}f(\phi)\phi\right], \tag{15}$$

as well as the functions

$$f_1 = \phi\frac{df}{d\phi} + f, \quad f_2 = -\sqrt{\frac{3}{16\pi G}}\frac{df_1}{d\phi} + f_1^2; \tag{16}$$

notice that this is no restriction on the potential shape. Then

$$\Phi = -\frac{3}{2}\lambda^2(\Omega_b\delta^b + \Omega_c\delta^c + 6X\varphi + 2X\varphi' - 2Y^2 f_1\varphi), \tag{17}$$

$$\Phi' = 3X\varphi - \Phi, \tag{18}$$

while the scalar field satisfies the equation

$$\varphi'' + \left(2 + \frac{\mathcal{H}'}{\mathcal{H}}\right)\varphi' + \lambda^{-2}\varphi - 12X\varphi + 4\Phi X + 2Y^2(f_2\varphi - f_1\Phi) = \beta\Omega_c(\delta^c + 2\Phi). \tag{19}$$

These expressions have been simplified by using the variables $X^2 = 8\pi G\rho_k(\phi)a^2/3\mathcal{H}^2$ (kinetic density parameter) and $Y^2 = 8\pi G V(\phi)a^2/3\mathcal{H}^2$ (potential density parameter). It follows that, if the DE kinetic (or potential) energy density gives a substantial contribution to the expansion source, X (or Y) is $\mathcal{O}(1)$.

In the Newtonian limit, however, we also neglect the derivatives of φ, averaging out the rapid oscillations of φ and the potential term $f_2 Y^2\varphi$; this actually requires that $\lambda \ll (f_2 Y)^{-1}$ [recall that Y is $\mathcal{O}(1)$]. Furthermore, in Eq. (19), the metric potential Φ, which is proportional to λ^2, can also be neglected. Accordingly, Eq. (17) becomes

$$\Phi = -\frac{3}{2}\lambda^2(\Omega_b\delta^b + \Omega_c\delta^c), \tag{20}$$

which is the usual Poisson equation, while Eq. (19) simplifies into

$$\lambda^{-2}\varphi \simeq \beta\Omega_c\delta^c. \tag{21}$$

In the same way (see [10]), we obtain the continuity equations

$$\delta^{c\prime\prime} = -\delta^{c\prime}\left(1 + \frac{\mathcal{H}'}{\mathcal{H}} - 2\beta X\right) + \frac{3}{2}\left(1 + \frac{4}{3}\beta^2\right)\Omega_c\delta^c + \frac{3}{2}\Omega_b\delta^b, \tag{22}$$

$$\delta^{b\prime\prime} = -\delta^{b\prime}\left(1 + \frac{\mathcal{H}'}{\mathcal{H}}\right) + \frac{3}{2}(\Omega_c\delta^c + \Omega_b\delta^b), \tag{23}$$

and the Euler equations

$$\theta^{c\prime} = -\theta^c\left(1 + \frac{\mathcal{H}'}{\mathcal{H}} - 2\beta X\right) - \frac{3}{2}\left(1 + \frac{4}{3}\beta^2\right)\Omega_c\delta^c - \frac{3}{2}\Omega_b\delta^b, \tag{24}$$

$$\theta^{b\prime} = -\theta^b\left(1 + \frac{\mathcal{H}'}{\mathcal{H}}\right) - \frac{3}{2}(\Omega_c\delta^c + \Omega_b\delta^b). \tag{25}$$

From the latter equations, we can derive the acceleration of a single nonrelativistic CDM or baryon particle (mass $m_{c,b}$), assuming that it lies in the empty space, at distance r from the origin, where either a CDM particle of mass M_c or a baryon particle of mass M_b is set.

In fact, owing to Eq. (10), normalizing the scalar field so that its present value $\phi_o = 0$, and assuming that the density of the particle is much larger than the background density, we get

$$\Omega_c\delta^c = \frac{\rho_{M_c} - \rho_c}{\rho_{crit}} = \frac{8\pi G e^{-\sqrt{16\pi G/3}\beta\phi}M_c\delta(0)}{3\mathcal{H}^2 a},$$

$$\Omega_b \delta^b = \frac{\rho_{M_b} - \rho_b}{\rho_{crit}} = \frac{8\pi G\,\delta(0)}{3\mathcal{H}^2 a},$$

δ being the Dirac distribution. Then, recalling that the divergence $\nabla_i v_i^{c,b} = \theta^{c,b}\mathcal{H}$, and using the ordinary (not conformal) time variable, instead of α, Eq. (24) yields

$$\dot{\nabla_i v_i^c} = -H(1-2\beta X)\nabla_i v_i^c - \frac{4\pi G^* M_c e^{-\sqrt{16\pi G/3}\beta\phi}\delta(0)}{a^2} - \frac{4\pi G M_b \delta(0)}{a^2}, \tag{26}$$

where the overdots indicate differentiation with respect to ordinary time,

$$G^* = G\left(1+\frac{4}{3}\beta^2\right) \tag{27}$$

and $H = d\log a/dt$.

We can integrate this equation, taking into account that the acceleration is radial, as the attracting particle lies at the origin. It will then be

$$\int d^3x \boldsymbol{\nabla}\cdot\dot{\mathbf{v}} = 4\pi\int dx \frac{d(x^2\dot{v})}{dx} = 4\pi x^2 \dot{v},$$

$\dot{v}$ being the modulus of the (radial) acceleration (in the second term $x = |\mathbf{x}|$). Accordingly, for a CDM particle, the desired expression of the radial acceleration reads

$$\dot{v}^c = -(1-2\beta X)H\mathbf{v}^c\cdot\mathbf{n} - \frac{G^* M_c e^{-\sqrt{16\pi G/3}\beta\phi}}{r^2} - \frac{GM_b}{r^2} \tag{28}$$

($\mathbf{n}$ is a unit vector in the radial direction; $r = ax$), which has various peculiarities and ought to be suitably commented on. To this end it is important to compare it with the radial acceleration

$$\dot{v}^b = -H\mathbf{v}^b\cdot\mathbf{n} - \frac{GM_c e^{-\sqrt{16\pi G/3}\beta\phi}}{r^2} - \frac{GM_b}{r^2} \tag{29}$$

of a baryon particle. In the expression (28), notice first the velocity term. This is a peculiar acceleration that exists even in the absence of particles displaying their attraction; its presence means that CDM is not expanding in a comoving way, due to the extra gravity it feels. Accordingly, its particles do not follow geodesics, because their mass changes in time, and their ordinary (not comoving) linear momentum obeys the equation

$$\dot{p_c} = -\frac{G^* M_c e^{-\sqrt{16\pi G/3}\beta\phi}}{r^2} - \frac{GM_b}{r^2}.$$

Baryon particles, instead, safely follow geodesics, although feeling that CDM particle masses are varying.

Let us conclude this section by summarizing its specific findings. (i) The mass assigned to CDM particles does vary in time, being $m_c = m_o e^{-\sqrt{16\pi G/3}\beta\phi}$, while baryon particles keep a constant mass. (ii) When interacting between themselves, CDM particles feel an effective gravitational constant $G^* = G(1+4\beta^2/3)$; any other particle-particle interaction occurs with the ordinary Newtonian interaction constant G.

IV. METHODS

Particle mass variations and different interaction constants ought to be taken into account in performing N-body simulations. They will be based on the adaptive refinement tree code (ART) [16] which has been suitably modified to deal with coupled DE models. The ART code starts with a uniform grid, which covers the whole computational box. This grid defines the lowest (zeroth) level of resolution of the simulation. The standard particle-mesh algorithms are used to compute density and gravitational potential on the zero-level mesh. The ART code reaches high force resolution by refining all high-density regions using an automated refinement algorithm. The refinements are recursive: the refined regions can also be refined, each subsequent refinement mesh of different resolution, size, and geometry covering regions of interests. Because each individual cubic cell can be refined, the shape of the refinement mesh can be arbitrary and can match effectively the geometry of the region of interest.

The criterion for refinement is the local density of particles: if the number of particles in a mesh cell (as estimated by the cloud-in-cell method) exceeds the level of n_{thresh}, the cell is split (''refined'') into eight cells of the next refinement level. The refinement threshold depends on the refinement level. For the zero level it is $n_{thresh} = 2$. For the higher level it is set to $n_{thresh} = 4$. The code uses the expansion parameter a as the variable time. During the integration, spatial refinement is accompanied by temporal refinement; namely, each level of refinement l is integrated with its own time step $\Delta a_l = \Delta a_o/2^l$, where $\Delta a_o = 3\times 10^{-3}$ is the global time step of the zeroth refinement level. This variable time stepping is very important for the accuracy of the results. As the force resolution increases, more steps are needed to integrate the trajectories accurately. Extensive tests of the code and comparison with other numerical N-body codes can be found in [22].

Let us now describe the three main modifications we made to handle coupled DE. The first step amounts to distinguishing between baryons and DM particles, which feel different gravitational forces. Therefore, the potential on the grid is to be calculated twice, to fix the different forces that the baryons and DM particles feel. All particles act on baryons through the usual gravitational constant G, which also sets the action of baryons on DM particles. DM particles, instead, act on DM particles through a different interaction constant $G^* = G(1+4\beta^2/3)$. The gravitational force is then computed through the usual fast Fourier transform FFT approach.

The second step amounts to taking into account that the effective mass of DM particles is time varying. Aside from the acceleration due to gravitation, each DM particle will

therefore undergo an extra acceleration $2\beta X$. In addition to these two changes, peculiar to coupled DE models, we ought to take into account the right relation between a and t, as shown in Eq. (11), where $\chi(a)=dt/da$ is given. By solving the background equations, in a suitable file we provide $\chi(a)$ for $\simeq 200$ scale factor values a_i, which we then interpolate.

The models listed in Table I were first simulated in a $80h^{-1}$ Mpc box. We then selected the same halo in all simulations and magnified it. The low-resolution simulation, performed with a force resolution of $15h^{-1}$ Mpc and a mass resolution $\simeq 2\times 10^{10}h^{-1}M_{\odot}$, allowed us to evaluate the halo mass function. The high-resolution simulation, performed with a force resolution of $\simeq 1.2h^{-1}$ kpc and a mass resolution of $2.54\times 10^{9}h^{-1}M_{\odot}$, magnified a sphere with a radius of $5h^{-1}$ Mpc, centered on the halo, allowing us to compare halo profiles down to a radius $\simeq 5h^{-1}$ kpc.

In addition to the above points, we could also test the nonlinear evolution of the *bias* between the amplitudes of inhomogeneities in baryons and DM. This bias is one of the most peculiar features of coupled DE models and we shall describe how nonlinearity modifies it.

V. RESULTS

A. Mass function

We identify halos in simulations by using a Spherical Overdensity (SO) algorithm, which we shall now describe in more detail. As a first step, candidate halos are located by a Friend of Friend (FOF) procedure, with linking length $\lambda = U\times d$ (d is the average particle separation) and keeping groups with more than N_f particles (U and N_f fixed below). We then perform two operations: (i) we find the point C_W where the gravitational potential, due to the group of particle, has a minimum; (ii) we determine the radius $\bar{r}$ of a sphere, centered in C_W, where the density contrast is Δ_v (we use the virial density contrast found in the absence of dark-dark coupling [13,23]). Taking all particles within $\bar{r}$ we again perform the operations (i) and (ii). The procedure is iterated until we converge onto a stable particle set. The set is discarded if, at some stage, we have fewer than N_f particles. If a particle is a potential member of two groups it is assigned to the more massive one. In this work we use $U=0.2$ and take N_f so as to have a mass threshold $5.0\times 10^{12}h^{-1}M_{\odot}$.

Figure 2 shows the mass function for isolated halos for models with different values of α and β. Let us recall that the simulations have the same initial phases and the same value $\sigma_8=0.75$. Thus, the differences between models are due only to different couplings or $w(t)$. Remarkably, at $z=0$ the mass functions are practically indistinguishable: a mass function has no "memory" of the past evolution. The mass function obtained in this way is well fitted by the approximation provided by [24] for ΛCDM models (long dashed line in Fig. 2).

B. Linear and nonlinear bias

From Eqs. (22),(23), the linear evolution of the density perturbations can be easily worked out (in some cases this can be done analytically [19]). In Fig. 3 we show $\delta^{c,b}$ as a function of the scale factor a.

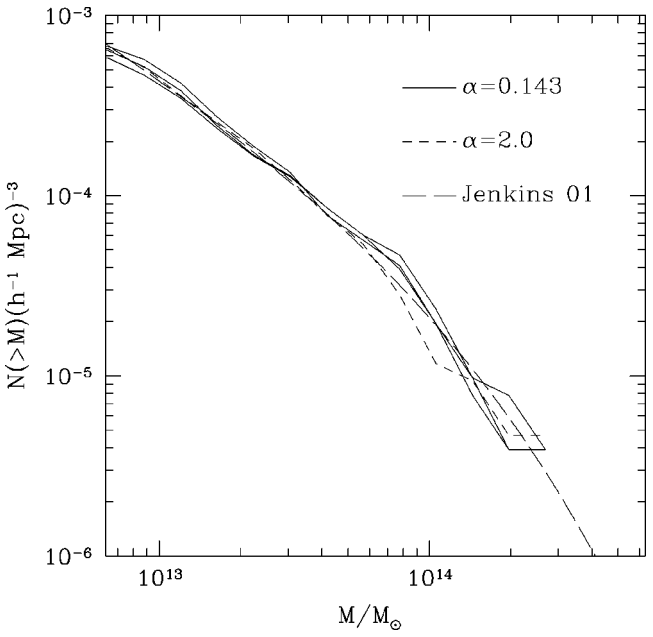

FIG. 2. Mass function at $z=0$ for $\alpha=2$ and $\alpha=0.143$. For $\alpha=0.143$ we report three curves, for different values of β. They are all practically indistinguishable and are well fitted by the approximation of [24].

As a consequence of these dynamical equations, δ^c develops a bias with respect to δ^b, due to the extra gravity felt by DM. At the present epoch, this bias, found in the linear theory, is well fitted by the following empirical expression:

$$b(\alpha,\beta)=\frac{\delta_o^b}{\delta_o^c}=\frac{1}{1+0.015\alpha\beta+2.1\beta^2}. \qquad (30)$$

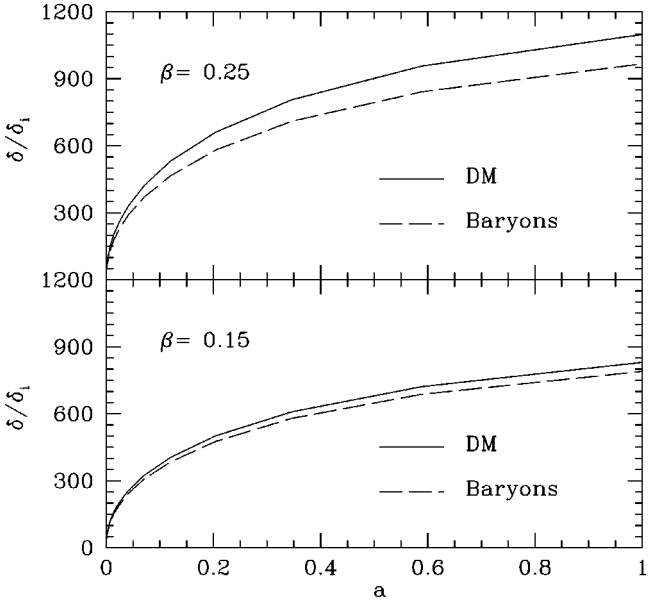

FIG. 3. DM and baryon linear perturbation growth for two different values of β. The dependence on α is weak and could not be appreciated in this plot.

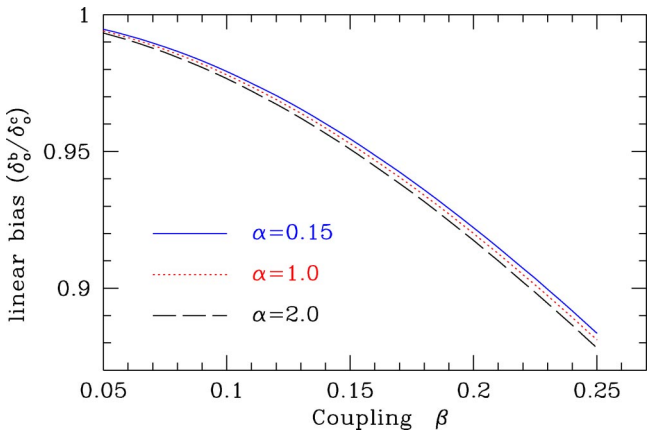

FIG. 4. Linear bias as a function of β for three values of α. Notice the very weak dependence on α.

Both this expression and Fig. 4 show that the bias b depends on β, while its dependence on α is very weak. Using the high-resolution clusters we can test the behavior of the bias in the highly nonlinear regime. To do so, we define the integrated bias B as

$$B(<r)=\frac{\rho_b(<r)-\hat{\rho}_b}{\hat{\rho}_b}\cdot\frac{\hat{\rho}_c}{\rho_c(<r)-\hat{\rho}_c},$$

where $\rho_c(<r)$ and $\rho_b(<r)$ are calculated inside a radius r from the halo center and we use a caret to denote average densities. In order to avoid problems with force resolution, the central zone ($r<10h^{-1}$ kpc) of the halo is not used. In Fig. 5 we show $B(<r)$ for the same halo, in cosmologies characterized by different coupling parameters β, keeping all other parameters equal. Figure 5 shows that nonlinearity significantly enhances the expected bias; however, at large scales, we recover the theoretical linear value, as provided by Eq. (30).

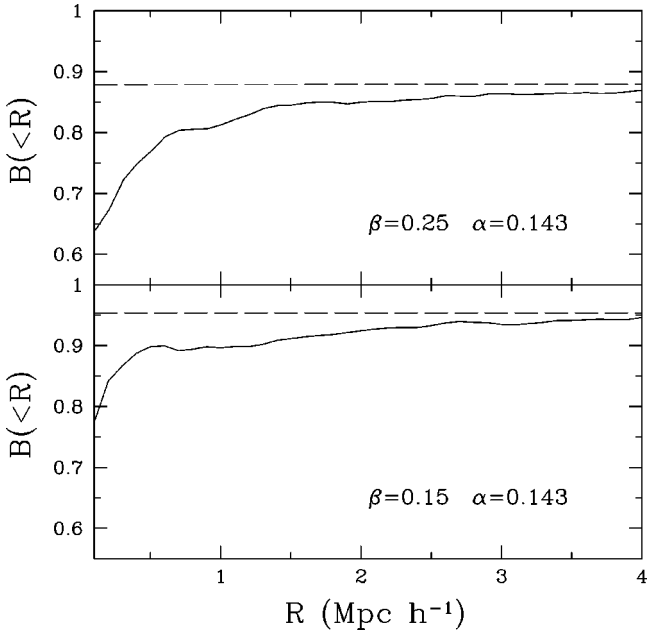

FIG. 5. Behavior of the integrated bias B for $\beta=0.15$ and for $\beta=0.25$. Notice that B tends to the predicted linear bias (dashed horizontal lines) at large scales.

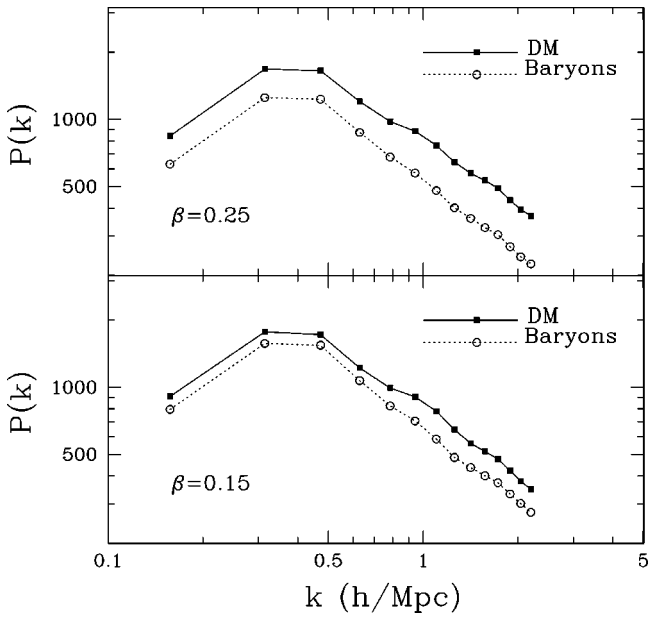

FIG. 6. Power spectra for DM and baryon particles evaluated from the simulations averaging over 60 random observers. The increase of the bias at small scales appears clearly.

The scale dependence of bias can also be appreciated from Fig. 6, where power spectra for baryons and DM, worked out from simulations at $z=0$, are shown.

C. Density profiles

Let us recall again that all simulations are started from the same random numbers. Therefore, it comes as no surprise that they yield similar world pictures. In the ΛCDM simulation, we selected a halo whose *virial* radius $r_v=812h^{-1}$ kpc encloses a mass $M_v=6.45\times10^{13}h^{-1}M_\odot$. Similar halos, located in the same place, are set in all other models considered. We then run new simulations of all models in Table I, magnifying the region centered on this halo. To do so, short waves were first added to the initial perturbation spectrum in all simulations.

In ΛCDM, the halo profile is accurately fitted by a Navarro-Frenk-White (NFW) expression [25,26]:

$$\frac{\rho(r)}{\rho_{cr}}=\frac{\delta^*}{(r/r_s)(1+r/r_s)^2}$$

with a scale radius $r_s=0.249h^{-1}$ Mpc (here ρ_{cr} is the critical density and δ^* is a parameter which sets the halo density contrast).

When the same halo is magnified in coupled DE models, we find model dependent behaviors toward the halo center. The essential restrictions to coupled DE models, arising from the nonlinear treatment, derive from these behaviors. However, in spite of such model dependence in the central areas,

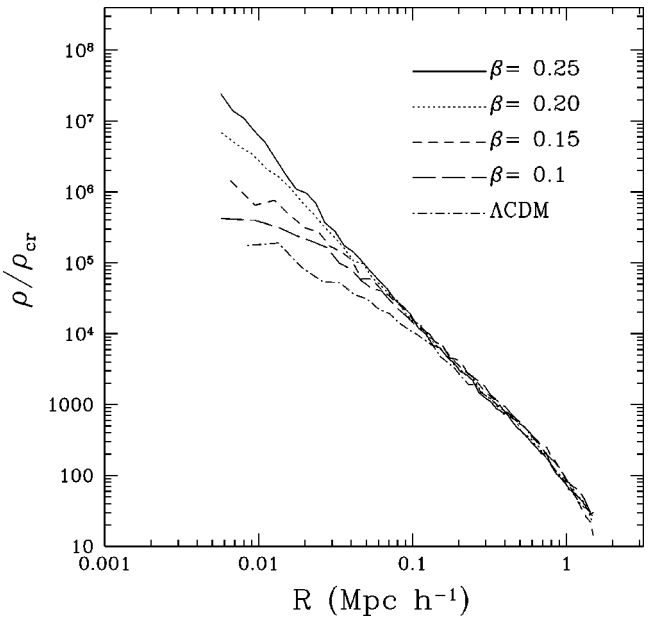

FIG. 7. DM density profile for four different coupling values and for ΛCDM.

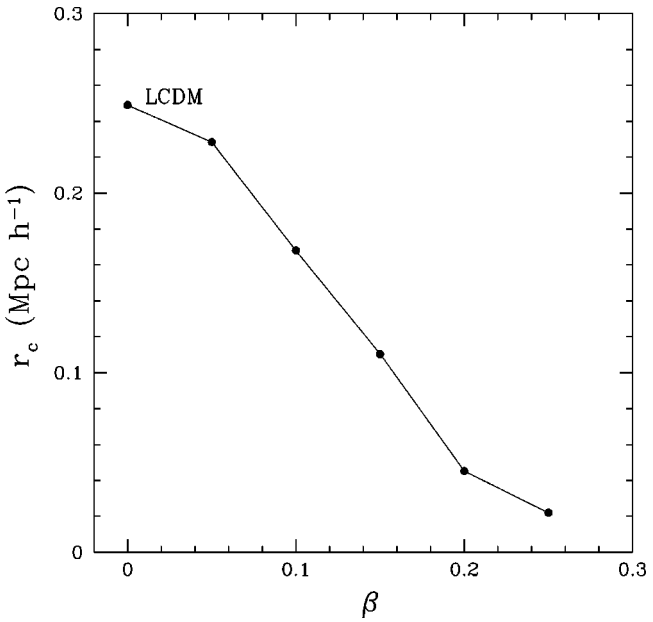

FIG. 8. Scale radius of a NFW profile as a function of the coupling parameter β.

the outer parts of the halos ($R > 100h^{-1}$ Mpc) show discrepancies that, from $100h^{-1}$ kpc to $700h^{-1}$ kpc, never exceed $\sim 10\%$.

Let us now discuss the substantial model dependence found in the central region ($R < 100h^{-1}$ kpc). It was already known that halos are denser in dynamical DE than in ΛCDM [14], although the density enhancement is fairly small and hardly exceeds $\sim 40\%$. Higher density means smaller r_s. The coupled DE simulations we performed show that the dark-dark coupling tends to enhance this effect. In Fig. 7 we overlap the profiles of the DM components of all our models, starting from ΛCDM (lower curve), up to a RP model with coupling parameter $\beta = 0.25$ (upper curve). The values of r_s change from $\simeq 0.25h^{-1}$ Mpc (ΛCDM) to $\simeq 0.022h^{-1}$ Mpc ($\beta = 0.25$). The dependence of r_s on β is plotted in Fig. 8.

In order to make sure that this effect was not related to some peculiarity of the halo selected, we magnified two other halos of a simulation with $\beta = 0.25$. Here we found even lower values for the scale radius r_s ($0.0105h^{-1}$ Mpc and $0.0103h^{-1}$ Mpc, respectively).

As a matter of fact, the profiles found for $\beta = 0.25$ or 0.2 can be fitted by a single power law:

$$\frac{\rho(r)}{\rho_{cr}} \propto r^{\gamma}$$

in the whole dynamical range, i.e., from $r = 1.0h^{-1}$ Mpc down to $r = 0.005h^{-1}$ Mpc (resolution limit), with a value of $\gamma \simeq -2.30$.

An analysis of Fig. 8 shows that only for β as low as $\simeq 0.1$ does r_s attain half the value for the ΛCDM. Accordingly, we may consider viable coupled RP models only with $\beta < 0.1$.

Simulations distinguish baryons from DM particles, as already discussed in the bias subsection. This allows us to draw separate density profiles. They are shown in Fig. 9, for two different coupled DE models (upper panel). No apparent discrepancy between DM and baryon profiles can be seen: they overlap fairly well, once we rescale them taking into account the different values of Ω_b and Ω_c (Fig. 9, lower panel).

In Fig. 10 we compare profiles of the same halo, with two different values of α (2.0 and 0.143), but with the same coupling ($\beta = 0.15$). The profiles overlap very well both for

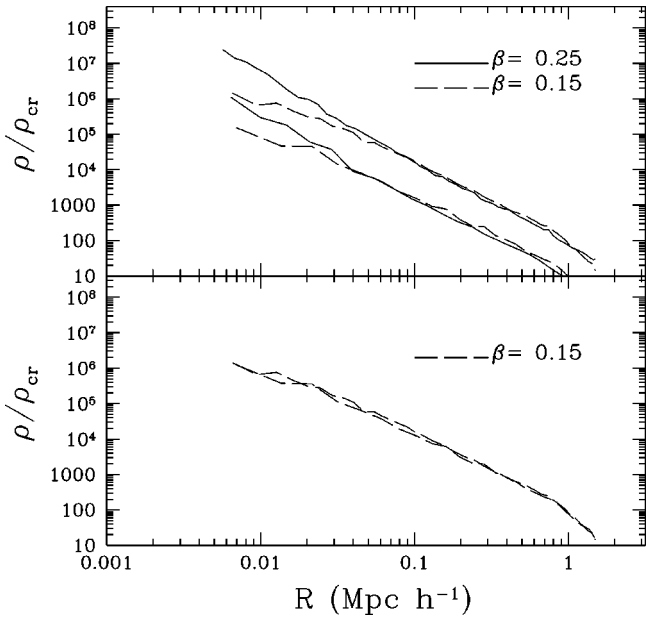

FIG. 9. Upper panel: DM and baryon density profiles (respectively, upper curve and lower curve) for $\beta = 0.15$ and for $\beta = 0.25$. Lower panel: once rescaled taking into account the different values Ω_b and Ω_c, there is no discrepancy between DM and baryons.

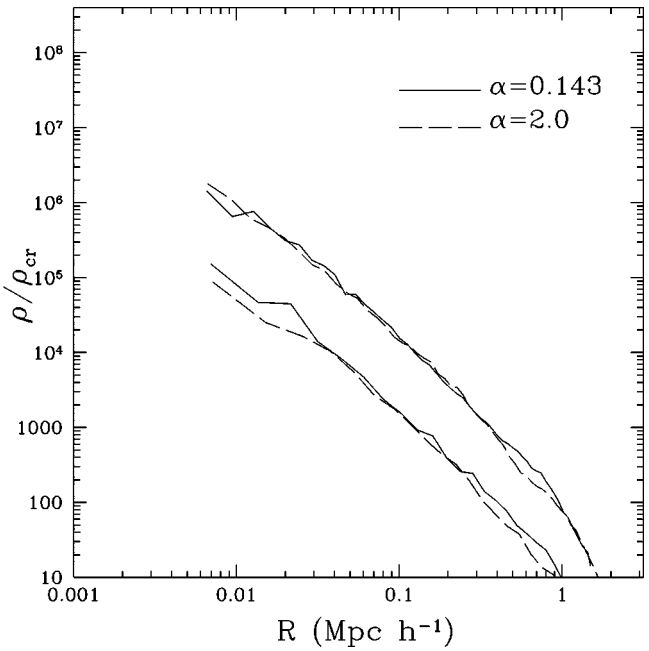

FIG. 10. DM and baryon density profiles for $\alpha=2$ and $\alpha=0.143$ (here $\beta=0.15$).

DM particles (upper curves) and for baryons (lower curves). We conclude that the slope of the profiles depends very weakly on α.

VI. CONCLUSIONS

After finding that coupled DE models are consistent with those observables whose behavior can be predicted at the linear level [3,4,10], a test of their nonlinear behavior had to be carried out. An optimistic hope was that coupled DE models helped to solve some of the long standing contradictions between observations and theoretical or numerical predictions (e.g., [27]). In particular, one could hope to find halo profiles whose shape is not NFW (if this is still a problem) with a slope distribution closer to the observed ones for low-surface-brightness galaxies [28,29] and spiral galaxies [30]. From this point of view, coupled DE with a RP potential leads to modest results. Very high coupling levels, instead of producing a flatter core, yield profiles still farther from observations. In all cases, the problem with the concentration distribution is not solved, just as when having recourse to models with (uncoupled) dynamical DE.

It should also be recalled that the RP potential considered here is characterized by very low α values. The scale factor dependence of the state parameter w, for such values of α, is shown in Fig. 1 and approaches -1 already at redshifts $\sim 3-4$. As far as the state parameter is concerned, therefore, these models are quite close to the ΛCDM and, in a sense, could be considered a variant of ΛCDMs, for which DE is coupled to DM.

In spite of the lack of improvement for what concerns slopes, *N*-body simulations lead to really significant results. First of all, the parameter space for coupled DE models is restricted to couplings $\beta<0.1$, but leaving wide room for significant couplings. Apart from the question of profiles, the halo mass function has been tested and found consistent with other DE models and with observations. Its evolution has been predicted and can be tested against future data. From this point of view, therefore, coupled DE passed the nonlinear test.

Performing *N*-body simulations was also important to test the evolution of the bias between baryon and DM fluctuations, which is one of the main characteristics of coupled DE models at the linear level. Here we showed that the bias still exists, and actually increases, in the nonlinear structures, and we studied its evolution. These results are open to an accurate comparison with data which will be deepened elsewhere.

Let us conclude these comments, however, with a further observation. Coupled DE apparently leads to higher halo concentrations essentially because of the evolution of the mass of DM particles and of the coupling constant between them. In the simulations we run, such mass depends on time and gradually decreases, as is predicted by coupled DE theories at the Newtonian approximation level. Accordingly, each DM particle mass was greater than today, in the past. Its gravity was therefore stronger. This is the reason why, although normalizing all models to the same σ_8 at $z=0$, we produce more concentrated halos: the forces which bound them were stronger in the past than today.

After appreciating this point, one can tentatively propose a way out for the halo concentration problem: a coupled DE model leading to DM particle masses which increase in time. This increase should also be fast enough to beat the higher gravity constant binding DM particles. This takes us back to the selection of a suitable self-interaction potential $V(\phi)$, which has no immediate obvious solution. This problem will therefore be studied more deeply in future work.

[1] A.G. Riess *et al.*, Astrophys. J. **116**, 1009 (1998); S. Perlmutter *et al., ibid.* **517**, 565 (1999).
[2] C. Bennet *et al.*, Astrophys. J. **583**, 1 (2003).
[3] L. Amendola and C. Quercellini, Phys. Rev. D **68**, 023514 (2003).
[4] L. Amendola, Mon. Not. R. Astron. Soc. **342**, 221 (2003).
[5] P.J. Steinhardt, L. Wang, and I. Zlatev, Phys. Rev. D **59**, 123504 (1999).
[6] L. Amendola, Phys. Rev. D **62**, 043511 (2000).
[7] M. Bento, O. Bertolami, and A. Sen, Phys. Rev. D **66**, 043507 (2002).
[8] B. Bassett, M. Kunz, D. Parkinson, and C. Ungarelli, Phys. Rev. D **68**, 043504 (2003).
[9] B.A. Gradwohl and J.A. Frieman, Astrophys. J. **398**, 407 (1992).
[10] L. Amendola and D. Tocchini-Valentini, Phys. Rev. D **66**, 043528 (2002).
[11] B. Ratra and P.J.E. Peebles, Phys. Rev. D **37**, 3406 (1988).

[12] T. Damour, G.W. Gibbons, and C. Gundlach, Phys. Rev. Lett. **64**, 123 (1990).
[13] R. Mainini, A.V. Macciò, S. Bonometto, and A. Klypin, Astrophys. J. **599**, 24 (2003).
[14] A. Klypin, A.V. Macciò, R. Mainini, and S. Bonometto, Astrophys. J. **599**, 31 (2003).
[15] E. Linder and A. Jenkins, Mon. Not. R. Astron. Soc. **346**, 573 (2003).
[16] A. Kravtsov, A. Klypin, and A. Khokhlov, Astrophys. J. **111**, 73 K (1997).
[17] P. Schuecker, R.R. Caldwell, H. Boehringer, C.A. Collins, and L. Guzzo, Astron. Astrophys. **402**, 53 (2003).
[18] T. Damour and K. Nordtvedt, Phys. Rev. Lett. **70**, 2217 (1993).
[19] L. Amendola, Phys. Rev. D **60**, 043501 (1999).
[20] C. Wetterich, Astron. Astrophys. **301**, 321 (1995).
[21] L. Amendola, M. Gasperini, D. Tocchini-Valentini, and C. Ungarelli, Phys. Rev. D **67**, 043512 (2003).
[22] A. Knebe, A. Kravtsov, A. Gottlober, and A. Klypin, Mon. Not. R. Astron. Soc. **317**, 630, 2003).
[23] R. Mainini, A.V. Macciò, and S. Bonometto, New Astron. **8**, 173M (2003).
[24] A. Jenkins *et al.*, Mon. Not. R. Astron. Soc. **321**, 372 (2001).
[25] J.F. Navarro, C.S. Frenk, and S.D.M. White, Mon. Not. R. Astron. Soc. **283**, L72 (1996).
[26] J.F. Navarro, C.S. Frenk, and S.D.M. White, Astrophys. J. **490**, 493 (1997).
[27] B. Moore, Nature (London) **370**, 629 (1994).
[28] W.J.G. de Blok and S.S. McGaugh, Mon. Not. R. Astron. Soc. **290**, 533 (1997).
[29] R.A. Swaters, B. Madore, F. van den Bosch, and M. Balcells, Astrophys. J. **583**, 732 (2003).
[30] A. Borriello and P. Salucci, Mon. Not. R. Astron. Soc. **323**, 285 (2001).